MARTIAN CRATER COUNTS ON ELYSIUM MONS, Kathleen McBride, Univ. of Houston-Clear Lake, 2700 Bay Area Blvd., Houston, Tx, 77058 and Lunar and Planetary Institute, 3303 NASA Rd. 1, Houston, Tx, 77058, and Nadine G. Barlow, SN 21, NASA Johnson Space Center, Houston, Tx, 77058.

Without returned samples from the martian surface, relative age chronologies and stratigraphic relationships provide the best information for determining the ages of geomorphic features and surface regions. We measured crater-size frequency distributions of six recently mapped geologic units of Elysium Mons to establish their relative ages [1,2].

Most of the craters on Elysium Mons and the adjacent plains units are between 500 and 1000 meters in diameter. However, only craters 1 km in diameter or larger were used because of inadequate spatial resolution of some of the Viking images and to reduce probability of counting secondary craters. The six geologic units include all of the Elysium Mons construct and a portion of the plains units west of the volcano. The surface area of the units studied is approximately 128,000 km^2. We used four of the geologic units to create crater distribution curves. There are no craters larger than 1 km within the Elysium Mons caldera. Craters that lacked raised rims, were irregularly shaped, or were arranged in a linear pattern were assumed to be endogenic in origin and not counted.

Three of the crater distribution curves (Figs. A,B,C) show that the ages of the surface units of Elysium Mons are near the heavy bombardment-post heavy bombardment transition. This is consistent with the ages found by Barlow [3]. These three units appear to have been emplaced at nearly the same time. The fourth curve (Fig. D) indicates that the upper flank material is slightly younger; this unit shows considerably fewer craters in the 1.0 to 2.8 km diameter size range. This lack of small diameter craters could have resulted from unusual erosion on the upper eastern flank of Elysium Mons or from the burial of the surface by a later volcanic deposit. In contrast to the undifferentiable, braided lava flows of the western flank, the upper flank is smooth and slightly hummocky at 150 m/pixel. A few craters appear mantled by some surficial deposit. The upper eastern flank has been interpreted as an ash deposit by Mouginis-Mark [4] and McBride and Zimbelman [2] because of its smooth, mantled appearing morphology.

Additional crater frequency distribution analysis is in progress and includes relative age chronologies for adjacent surface units, west of Elysium Mons, to determine the geologic history of Elysium Mons.

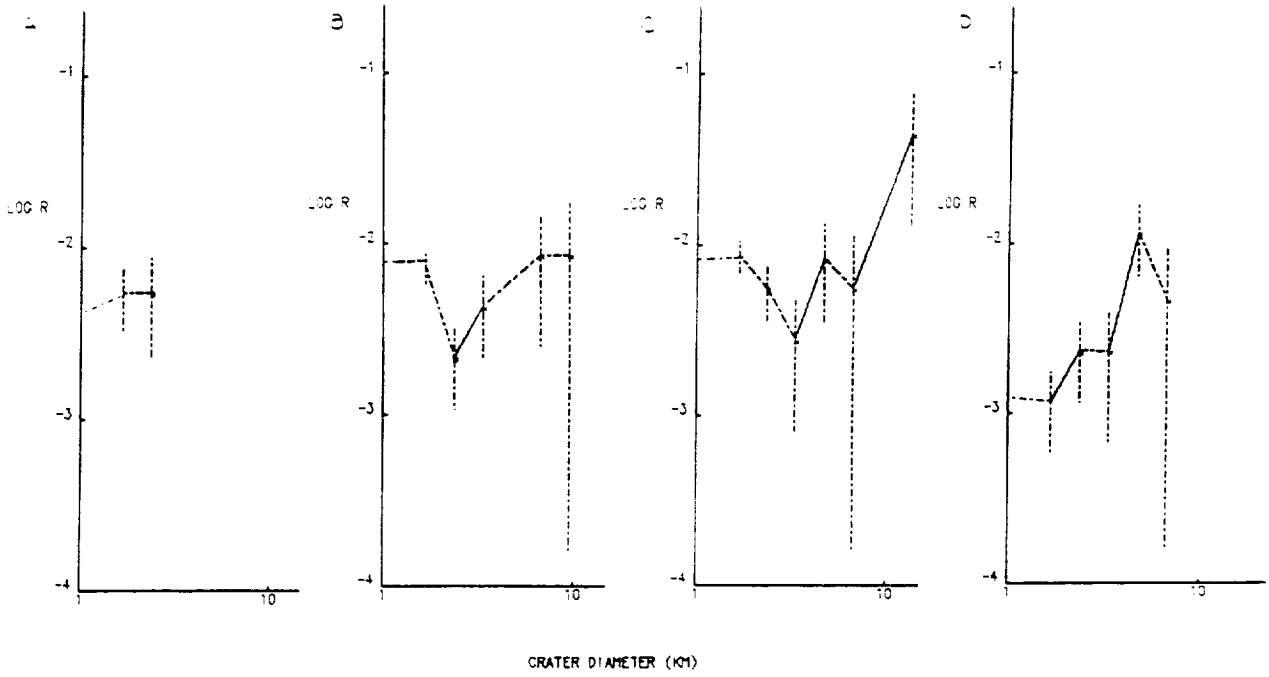

Figures: Relative crater-size frequency distribution curves. (A) Lower/Middle Flank Material. (B) Undifferentiated Flow Material. (C) Plains Unit. (D) Upper Flank Material.

REFERENCES: [1] McBride et al., LPI Tech. Rpt., 89-04, p. 56-58, 1989. [2] K. McBride and J. R. Zimbelman, LPSC 20, p. 651, 1989. [3] N. G. Barlow, Icarus 75, p. 285-305, 1988. [4] P. J. Mouginis-Mark, LPSC 12, p. 726-728, 1981.

DEVELOPMENT OF THE SOUTHWEST ELYSIUM CANYON COMPLEX, MARS; J.H.McDonnell, Consulting Geologist, 5400 Las Trampas Way NW, Albuquerque, New Mexico 87120

A photogeologic study of a large system of depressions (1) on Mars, 320 kilometers west of Elysium Mons (2,3,), reveals component structures of varying age and morphology (1). This system, referred to as the Southwest Elysium Canyon Complex, is one of a number of large depressions found west of Elysium Mons and is distinct in its orientation and form.

Analysis involved stereoscopic and low magnification study of Viking Orbiter images at scales ranging from near 3 km/cm. to about 18 km/cm. and photomosaics at 1:2 million and 1:500,000. Descriptions were made along with measurements and overlay maps. Classification, evolutionary sequence, and genetic interpretations follow.

The Southwest Elysium Canyon Complex comprises the Elysium Chasmata, Hyblaeus Chasma, Stura Vallis, and certain Elysium Fossae (4), along with various pits and graben. The complex is dominated by the Elysium Chasmata and related fosae which provide the predominent NNW-SSE orientation and near 240 kilometer overall length. The overall width is variable, around 30 to 50 kilometers. Individual components, for the most part, range from less than five to 15 kilometers across.

The Elysium Chasmata and related fossae are a series of large, deep, elongate depressions which trend N36W to N20W, more or less tangentially to Elysium Mons, but which become radial at the extreme north end. Hyblaeus Chasma and Stura Vallis, on the other hand are broad, shallow depressions which align radially to Elysium Mons, normal to the Elysium Chasmata. A fossa at the north end of the complex is also radial to Elysium Mons.

All more or less linear depressions having discernible widths are considered fossae. Their classification is based on form (1,5), distinguishing characteristics, and inferred genesis. Chasmata in this instance are simply larger versions and do not represent a distinct morphologic class. All fossae here are closed (1,5). Within this division they are classified as being either floored or floorless (1). Floored fossae have wide smooth floors, steep sides, and somewhat trapezoidal cross sections. Floorless fossae have sloping interiors and rounded, U-shaped, cross sections. Elysium Chasmata and related fossae are floorless. Hyblaeus Chasma and Stura Vallis on the south and certain fossae at the north end of the complex are floored. This contrast follows orientation, and inferred relative age and genesis.

Elysium Chasmata and related fossae are some of the youngest features in the region and are the deepest components of the complex. They intersect and displace virtually all features encountered. The northernmost projection down drops the floor of the northern radial floored fossa. Deep northern fossae slice across shallower, floored fossae which trend in nearly the same direction. The southernmost chamsa cuts of the ends of Hyblaeus Chasma and Stura Vallis, and is depressed well below them.

SOUTHWEST ELYSIUM CANYON COMPLEX: McDonnell, J.H.

Both of the southern chasmata follow and truncate intersecting arcuate graben (3), which are also found along side them.

The radial, floored fossae are older, but not necessarily the oldest structures. The floor of Hyblaeus Chasma is off set by graben, while the rim in stepped back between faults; suggesting the graben are older, but have seen successive movement. Conversely, the chasma may have down dropped differentially between faults in the manner of rim set back. Hyblaeus structurally off sets near by pits, making the latter older. But others are inferred to be younger or penecontemporaneous on the basis of convexity of separating wall.

Aligned, floorless pits at the northeast end of the complex are among the oldest depressions. They are intersected by the northern radial fossa which has dropped below them. Fossae on the northwest and opposedly concave east are thought to be intermediate in age as they tend to be shallow and floored and are intersected by more recent fossae. Finally the long gouge-like fossa west of the Elysium Chasmata, between Hyblaeus and the northern fossae, is inferred to be penecontemporaneous with the Elysium Chasmata. It also intersects and cuts through all features encountered.

In summary, the depressions which make up what is called the Southwest Elysium Canyon Complex show a decided dichotomy in form and orientation and a definite sequence of formation. All are topographically closed (1,5) and are otherwise characterized by the presence or absence of well discernible floors. Graben and some pits are early, followed by radial and other floored fossae. These latter developed either as graben or by subsidence along irregular lines of weakness. Most recent are the deep floorless fossae running diagonally to Elysium Mons, which have developed along the earlier graben. The problem of material removal remains, but the draining and collaps of large shallow magma chambers (6) may be called for along with the interaction of near surface ice (1).

References

(1) Mouginis-Mark, P.J.(1985), Icarus 64, 265-284.
(2) Malin, M.C.(1977) GSA Bull. V.88, 908-919.
(3) Tanaka, K.L., Scott, D.H.(1985) Geologic Map of the Elysium Region of Mars, U.S.Geolgoical Survey Miscellaneous Investigation Series Map I-xxxx, Version 10/8/85.
(4) U.S. Geological Survey (1985), MTM-20217 &25217, Atlas of Mars, 1:500,000 topographic series.
(5) Sharp, R.P., Malin, M.C.(1975) GSA Bull. V.86, 593-609.
(6) Decker, R., Decker, B.(1981) Volcanoes, W.H.Freeman & Co.

VALLES MARINERIS LANDSLIDES: EVIDENCE FOR MECHANICS OF LARGE ROCK AVALANCHES; A. S. McEwen, U. S. Geological Survey, Flagstaff, AZ 86001.

The mechanism of transport of large rock avalanches has been the subject of considerable interest and controversy in recent decades. On Earth, the observed runout lengths (L) for large rock avalanches, relative to the height of drop (H), are much greater than can be explained by either sliding or dispersive grain-flow mechanisms. Most natural rock types have coefficients of friction (either sliding or internal friction) of 0.6 or higher, so movement is expected only over terrain with an average slope of at least 30° (or H/L at least 0.58); this expectation is confirmed for rock avalanches of relatively small volume and for other flows of dry, granular material. However, as rock avalanches increase in volume, H/L decreases to values as low as 0.1 or less, and a log-log plot of H/L versus volume shows a linear correlation [1,2].

Planetary comparisons under different conditions of gravity, atmospheric pressure, and volatile inventory may prove essential to resolving this question of mechanism. Mars is the only planetary body other than Earth known to have long-runout landslides; they are abundant in the equatorial canyon system of the Valles Marineris. Were the Valles Marineris landslides "wet" or "dry"? ("Wet" is taken to mean that the mass was saturated with water, thus eliminating or greatly reducing grain-to-grain contacts.) Lucchitta [3] thought that they were probably wet, whereas McEwen [4] concluded that they were probably dry. It has even been suggested that the landslides were subaqueous, collapsing into lakes [5]. However, the landslides are among the geologically youngest features on Mars [6]; they clearly postdate the interior layered deposits (of possible lacustrine origin), and there is no evidence for liquid water on the surface of Mars at the time of their formation.

Landslide properties were measured in three regions of Valles Marineris, where 1:500,000-scale topographic maps with 200-m contour intervals are available: (1) the Tithonium and Ius Chasmata region from about lat -9° to -4°, long 83° to 88° [7]; (2) an additional part of Tithonium Chasma from lat -7.5° to -4°, long 80° to 85°; and (3) a region including Ophir Chasma and part of Candor Chasma from lat -7.6° to -3°, long 70° to 75.1°. (Work on maps of the last two regions is in progress by the U.S. Geological Survey.) Within these regions, 25 landslides having identifiable source locations and avalanche deposits were studied. All of the relatively high resolution (200 m/pixel or better) Viking Orbiter images of these areas were utilized.

Landslide volumes were estimated by two methods. For the large landslides with well-defined slump scars, the volume missing from the scars was estimated. For the smaller landslides, the scars are too small relative to the topographic data for the missing volume to be estimated, but the deposits appear to have uniform thicknesses; thus the volumes were estimated from the landslide-deposit area times the estimated height of the flow front. The errors in the volume estimates are small compared

with the variations in landslide volume (more than 5 orders of magnitude.

If we assume a Bingham rheology for the avalanche and uniform, steady flow conditions, then the yield strength, K, may be estimated by $K = pgDsin\beta$, where p is the flow density, g is the gravitational acceleration (3.72 m/s for Mars), D is the height of the flow front, and ß is the ground slope at the flow front. For p, 2000 kg/m^3 was assumed, which is characteristic of terrestrial rock avalanches. Yield-strength estimates range from 10^4 to 10^5 Pa. Terrestrial dry-rock avalanches are characterized by yield strengths near 10^4 Pa, whereas water-saturated debris flows have yield strengths typically from 10^2 to 10^3 Pa. Therefore, even with an uncertainty in the yield-strength estimates of an order of magnitude, the values are clearly consistent with the yield strengths typical of dry rock debris.

Trends of decreasing H/L with increasing volume are obvious from both the terrestrial and the Valles Marineris observations. Least-square fits to the datasets give linear correlation coefficients of 0.82 for the terrestrial points and 0.90 for the Valles Marineris points. The slopes of the two trends are nearly identical. These relations are very different from those seen in wet debris flows, where H/L is almost always less than 0.1 irrespective of volume. If the Valles Marineris landslides were either wet debris flows or subaqueous flows, then the points would be expected to plot below the terrestrial values for dry rock avalanches. Instead, the Valles Marineris trend plots above the terrestrial trend.

Although the slopes of the terrestrial and Valles Marineris trends are nearly identical, there is clearly an offset between the trends. At a given value of H/L, the Martian landslides are typically about 50 to 100 times more voluminous than the terrestrial counterparts, or, at a given volume, H/L is typically about two times larger on Mars. The offset might be explained by the effect of a lower g on flows with high yield strengths. Although this explanation does not answer the more fundamental question of how friction is overcome in large dry-rock avalanches, it does suggest that the correct model should be consistent with the presence of high yield strengths in the moving flows. Fluidization by a gas, for example, eliminates the yield strength in an active flow and is not consistent with the evidence presented here.

[1] Scheidegger, A. E., 1973, Rock Mechanics 5, 231-236.
[2] Hsu, K. J., 1975, Geol. Soc. America Bull. 86, 129-140.
[3] Lucchitta, B. K., 1987, Icarus 72, 411-429.
[4] McEwen, A. S., 1989, Geology 17, 1111-1114.
[5] Shaller, P. J., Murray, B. C., and Albee, A. L., 1989, Lunar and Planetary Science XX, 990-991.
[6] Lucchitta, B. K., 1979, J. Geophys. Res. 84, 8097-8113.
[7] U. S. Geological Survey, 1980, Misc. Inv. Ser. Map I-1294.

POLYGONAL TERRANE OF MARS: STRESSES FROM DRAPE FOLDING, George E. McGill and L. Scott Hills, University of Massachusetts, Amherst, MA 01003.

The giant polygons of Acidalia and Utopia planitiae pose a fascinating mechanical problem: all of the earth analogues that come readily to mind are almost certainly invalid. Polygonal structures on the earth demonstrate a roughly 10:1 relationship between polygon diameter and the depth of the bounding fractures (1). Transferring this relationship to the giant polygons of the martian northern plains, which are 5-20 Km in diameter, requires that fracturing driven by cooling or desiccation penetrate to depths as great as 2 Km. This is mechanically unlikely, as is convincingly argued by Pechmann (2), who concludes that only deep-seated tectonic stresses could account for the fracture depth required to form such large polygons. But the giant martian polygons do not resemble any known tectonic structures (2,3). Polygonal terrane corresponds in age to large outflow channels that drain from the highlands into the lowlands (4), and it occurs in the topographically lowest parts of the lowlands (5). It also can be shown that the polygonal troughs formed almost immediately following deposition of these materials (3), a timing that does not rule out a tectonic origin, of course, but which does strongly suggest a link between deposition and fracturing. Geological evidence thus favors a model for polygon formation that involves shrinkage stresses due to desiccation of wet sediment. However, most similar structures on earth have dimensions on the order of centimeters to meters; rare large polygons with diameters up to 300m are known from a few playas (6).

The martian polygonal terrane was deposited unconformably on top of a rugged surface characterized by knobs, mesas, fragments of ancient crater rims, and scattered fresh craters (3,7). This rugged surface is exposed south of the polygonal terrane of Utopia planitia. Northward, the surface is increasingly obscured by younger plains deposits until it disappears completely beneath polygonal terrane (7). Circular troughs present among the more irregularly shaped polygons within polygonal terrane occur above buried fresh craters similar to those exposed to the south. The complete burial of a crater population that includes craters as large as 40 Km in diameter requires that polygonal terrain be at least 450m thick (8). Moreover, the sediments also must be thick enough to cover the crater rims to depths greater than the apparent depths of the circular troughs, implying a thickness on the order of 600m. The presence of rugged topography beneath a thick layer of wet sediment will result in the development of drape anticlines and synclines as the sediment compacts because the total downward displacement of an originally horizontal plane within the sediments will vary directly with the thickness of compacting underlying material. These drape folds will superpose bending stresses onto the pervasive tensile stresses due to desiccation shrinkage. The objectives of this research are 1) to test the feasibility of this model by estimating the magnitudes of the stresses involved, and 2) to continue developing an hypothesis for polygon formation that considers both geological and mechanical data.

Because crater morphology is well known (8), and because of the geometric simplicity provided by radial symmetry, our mechanical analysis considers the specific case where the rim of a crater 10 km in diameter is covered by sediments thick enough to bury the rim to a depth of 400m. For purposes of analysis, it is convenient to consider the lower part of the sedimentary layer filling the crater as an "older fill", and the upper part as a "younger cover". This may actually represent the true geological history of the deposit, but the analysis does not depend on this.

Two quantitative models are attempted, one based on plate-bending theory, the other using finite-element methods. Both models draw on the literature of soil mechanics to estimate the rheological properties of polygonal terrane materials. Most normally consolidated sand- and clay-rich soils exhibit Young's moduli in the range 5-75 MPa, and Poisson's ratios between 0.25 and 0.40 (9). Cohesive strengths commonly are negligible, and shear failure is governed by angles of internal friction averaging 30°. The plate bending model considers all material above the crater rim to be an elastic plate that is bent as the underlying older fill compacts under the load of the younger cover. Because boundary conditions impose a sinusoidal shape on the bent plate, this

approach does not predict a very realistic shape for a drape fold formed over the upward-concave slope of a crater wall. However, the sinusoidal shape underestimates bending stresses, and thus is conservative. The finite-element model considers the three-dimensional elastic deformation of older fill and younger cover as a function of position and time. The buried crater rim is modeled using a cubic spline, hence the shape of the resulting drape fold seems very realistic. Because of the flexibility of the finite-element method, various depth-dependent combinations of elastic properties and extent of preconsolidation can be modeled. The assumption of purely elastic compaction, although probably not very realistic, also is conservative.

The two approaches yield similar results. Even when very conservative estimates of compaction of older fill are used (<10%), failure by brittle fracture or by shear is predicted to depths of the right order to account for the troughs bounding the martian polygons. This result is obtained without considering the tensile stresses due to desiccation shrinkage. If these are of the same order as the bending stresses, as seems likely, then not only are the total stresses available adequate to cause failure to the requisite depth, but superposition of these two stress systems will produce significant differences in total tensile stresses available to initiate fracturing at the surface; the probability of fracturing will be enhanced by drape anticlines and domes above crater rims and knobs/mesas, and suppressed by drape synclines between these features. Thus the scale of the polygons relates to the spacing of buried topographic features rather than to the strength/thickness characteristics of the sediment layer.

Compaction and bending must occur quickly enough for elastic strains to build up faster than they can be relaxed by pseudoviscous creep. Equivalent viscosity of soil is rarely determined, but in slow landslides it is estimated to be about 10^5-10^6 MPa-s (10). Maxwell times for materials with equivalent viscosities of 10^6-10^8 MPa-s and Young's moduli of about 10 MPa are months to years. Very large Maxwell times (order of 10^6 years) would thus seem to require unrealistically high equivalent viscosities. Consequently, it appears as if the formation of the martian polygons must be a geologically rapid process.

(1) Lachenbruch, A.H., J. Geophys. Res., 66, 4273-4292, 1961.
(2) Pechmann, J.C., Icarus, 42, 185-210, 1980.
(3) McGill, G.E., Geophys. Res. Letts., 13, 705-708, 1986.
(4) Neukum, G., and K. Hiller, J. Geophys. Res., 86, 3097-3121, 1981.
(5) Lucchitta, B.K., et al., J. Geophys. Res., 91, E166-E174, 1986.
(6) Neal, J.T., , et al., Bull. Geol. Soc. America, 79, 69-90, 1968.
(7) McGill, G.E., J. Geophys. Res., 94, 2753-2759, 1989.
(8) Pike, R.J., and P.A. Davis, Lunar Planet. Sci. XV, 645-646, 1984.
(9) Hunt, R.E., Geotechnical Engineering Analysis and Evaluation, McGraw-Hill, 1986.
(10) Iverson, R.M., in Abrahams, A.D., Hillslope processes, Allen & Unwin, 1986.

STATE OF STRESS AND ERUPTION CHARACTERISTICS OF MARTIAN VOLCANOES. Patrick J. McGovern and Sean C. Solomon, Dept. of Earth, Atmospheric, and Planetary Sciences, Massachusetts Institute of Technology, Cambridge, MA 02139.

Introduction. The growth of a large volcano exerts a load on a planetary lithosphere that can give rise to flexural deformation and faulting. Lithospheric stress, in turn, can influence the state of stress within the volcano and thus the characteristics of eruptions and the deformation and growth of the construct. Previous studies of the stress state within and beneath terrestrial volcanoes have been of two main types: (1) models of plate flexural stresses in isolation [1,2], or (2) finite element models of volcanic bodies with rigid lower boundary conditions [3,4]. We seek a model which couples the stress and displacement fields of both the plate and volcano structures, in order to understand the behavior of Martian volcanoes and the relationship of eruption styles to evolving local and regional stress.

Method. We use the finite element code TECTON, written by H.J. Melosh and A. Rafesky [5,6], to construct axisymmetric models of volcanoes resting on an elastic lithospheric plate overlying a viscoelastic asthenosphere. This code can model buoyancy forces supporting the plate, thus allowing a proper representation of plate flexure. Several values of the ratio of volcano size to lithospheric thickness were considered. The thickness of the strong upper lithosphere was taken from flexure models [7]. The viscoelastic layer was taken to extend to a sufficient depth so that a rigid lower boundary has no significant influence on the results. The code first calculates elastic deformations and stresses and then determines the time-dependent viscous deformations and stresses. Time in the model scales as the Maxwell time in the asthenosphere.

Results. The deviatoric stress field (principal stress directions) resulting from the elastic deformation induced by a volcano 20 km in height and 400 km in diameter on a strong lithosphere 40 km thick (parameters appropriate to Ascraeus Mons) is shown in Fig. 1. The stress field after the plate has flexed under the volcanic load is shown in Fig. 2. We note two effects of plate flexure with increasing time: (1) the deviatoric stresses in the surface region grow quite large; and (2) the area where the principal compressive direction is parallel to the surface extends progressively deeper, eventually reaching into the crust beneath the construct. Also, at large times, the boundary between the area of rotated stress directions and the underlying area of 'normal' stress orientations (compression axis vertical) is a region of low deviatoric stress. We find that plate deflections and stresses within the lithosphere are in qualitative agreement with those of flexural models [7].

Discussion. The above effects of flexure on the volcano stress field may have important implications for the history of volcanic events. It has been suggested [1] that time-dependent flexural stresses at the top of the elastic lithosphere beneath the Hawaiian volcanic chain control the history of eruptions at individual volcanoes, with eruptions ceasing during intervals when the two principal horizontal stress deviators are compressive and of significant magnitude. Applied to our model, this would imply that at early times after an interval of significant shield-building eruptions, the horizontal stress deviators within and beneath the volcano are tensional, so magma ascent to high-level chambers within the construct is favored. At later times, the stress directions in and beneath the volcano rotate such that the most compressive axis is nearly horizontal, so high-level magma bodies and summit eruptions would not be expected unless the ascending magma is significantly overpressured. In contrast, given that magma propagates through conduits oriented perpendicular to the least compressive stress, the stress orientations shown in Fig. 2 imply that flank eruptions are preferred at this stage of development. The young ages of the volcanic units surrounding Olympus Mons and Tharsis Montes are consistent with such an evolution in eruptive style [8].

Conclusions. These initial models suggest that the state of stress during volcano growth and lithospheric flexure can have an important influence on volcano evolution on Mars. Further models are planned to examine the roles of magma chamber overpressure and evacuation and near-surface faulting on the stress orientations presented here.

References. [1] U.S. ten Brink and T.M. Brocher, *JGR, 92,* 13687, 1987; [2] C.H. Thurber and A.E. Gripp, *JGR, 93,* 4721, 1988; [3] L. Chevallier and W.J. Verwoerd, *JGR, 93,*

4182 1988; [4] J.H. Dieterich, *JGR, 93,* 4258, 1988; [5] H.J. Melosh and A. Rafesky, *GJRAS, 60,* 333, 1980; [6] H.J. Melosh and A. Rafesky, *JGR, 88,* 515, 1983; [7] R.P. Comer et al., *Rev. Geophys., 23,* 61, 1985; [8] D.H. Scott and K.L. Tanaka, *Icarus, 45,* 304, 1981.

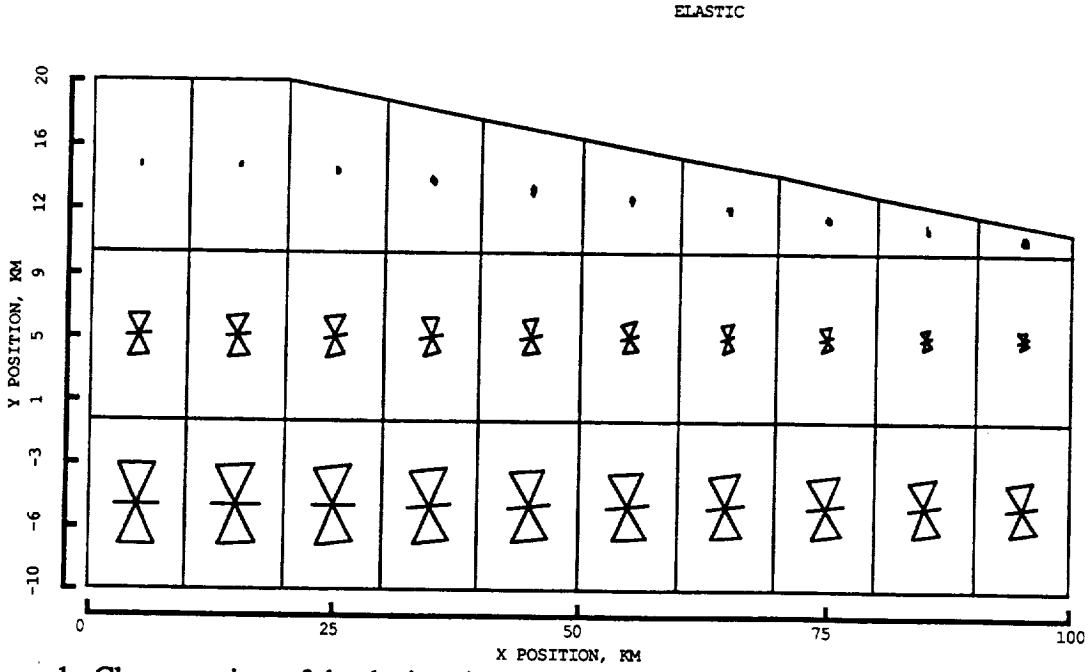

Figure 1. Close-up view of the deviatoric stress field in the volcano after the initial elastic deformation. An hourglass shape denotes the principal axis of compression, a bar denotes the principal axis of tension; the size of each symbol is proportional to deviatoric stress magnitude. The axis of rotational symmetry is x=0.

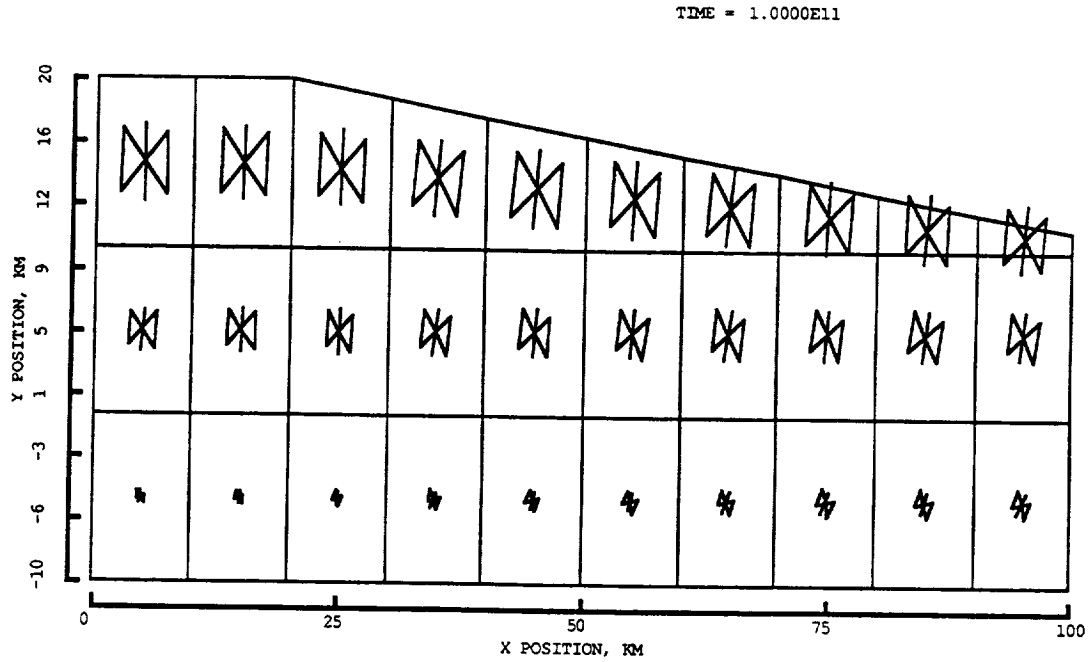

Figure 2. Deviatoric stress field in the volcano after flexure. The time elapsed is on the order of 100 Maxwell times. Rotation of the stress axes extends downward to the top layer of the plate (below y=0).

ANALYSES AND MORPHOLOGY OF A LAVA FLOW, ASCRAEUS MONS, MARS; H.J. Moore, U.S. Geological Survey, Menlo Park, CA, 94025 and P.A. Davis, U.S. Geological Survey, Flagstaff, AZ, 86001.

We have obtained some 32 profiles of lava flows on Mars using photoclinometry [1]. These photoclinometric profiles were leveled by adjusting them until the levee crests had the same elevations. Here, we compare our lava-flow dimensions and rheologic analyses for one profile on Ascraeus Mons with previous results using dimensions from images and shadow techniques [2, profile E5] (fig. 1, Table 1). In our rheological analyses, we use a wide-flow model [3], Hulme's model [4], and model 1 of Baloga and Crisp [5]. Effusion rates are estimated by using an unmixed-cooling model [6] and calibrated by using Hawaiian flows [7] and a Graetz-number model [4,8]. Our Graetz-number effusion rates are about 3.9 times larger than previous ones [7] because of a corresponding increase in thermal diffusivity.

In general, our results are compatible with the previous ones [2] (Table 1). Yield strengths are about 1 to 10 kPa, and Bingham viscosities are about 1 to 10 MPa*s. Newtonian viscosities for the wide-flow model are about 4 times larger than Bingham viscosities. Rates of shear are very small (5×10^{-8} s^{-1}). Both Newtonian viscosities and rates of shear are comparable to those expected for basaltic flows just before they stop [9,10].

Morphologies of flow E (fig. 1) and of many other flows near the summit of Ascraeus Mons are complex and similar to those of Hawaii [11] and Etna [12]. For both types of flows, morphologies indicate the presence of overflow levees, sheets, and lobes, breached lava ponds and breakouts; locally, channels appear clogged (profile A, fig. 1) and, in other places, drained (profile B, fig 1); and tips of flows are commonly multilobed (fig. 1). Interpretation of these flows introduces uncertainties into the appropriate flow dimensions to be used in the rheologic models. Additional uncertainties exist that are related to effusion-rate models and parameters, flow lengths and areas, and measurement techniques. Thus, the compatibility of the results from our rheologic analyses and the previous results [2] is surprising.

REFERENCES

[1] Davis, P.A., et al., 1984, J. Geophys. Res., v. 89, p. 9449-9457. [2] Zimbelman, J.R., 1985, J. Geophys. Res., v. 90, Suppl. D, p. D157-162. [3] Moore, H.J., et al., 1975, Proc. 6th LSC., p. 101-118.. [4] Hulme, G., 1974, Geophys. J. Roy. Astron. Soc., v. 39, p. 361-383. [5] Baloga, S.M. and Crisp, J., 1988, unpubl. rept., 35 p. [6] Pieri, D.C., et al., 1986, J. Volc. Geotherm. Res., v. 30, p. 29-45. [7] Moore, H.J., et al., 1989, Repts. Planet. Geol. Geophys. Prgm.-1988, NASA TM 4130, p. 387-389. [8] Hulme, G., et al., 1977, Phil. Trans. Roy. Soc., Lond., ser. A, v. 285, p. 227-234. [9] Moore, H.J., 1987, USGS Prof. Paper 1350, p. 1569-1588. [10] Walker, G.P.L.,

1967, Nature, v. 213, p. 484-485. [11] Lipman, P.W., et al., 1987, USGS Prof. Paper 1350, p. 1527-1567. [12] Kilburn, C.R.J., et al., 1988, J. Geopys. Res., v. 93, p. 14759-14772.

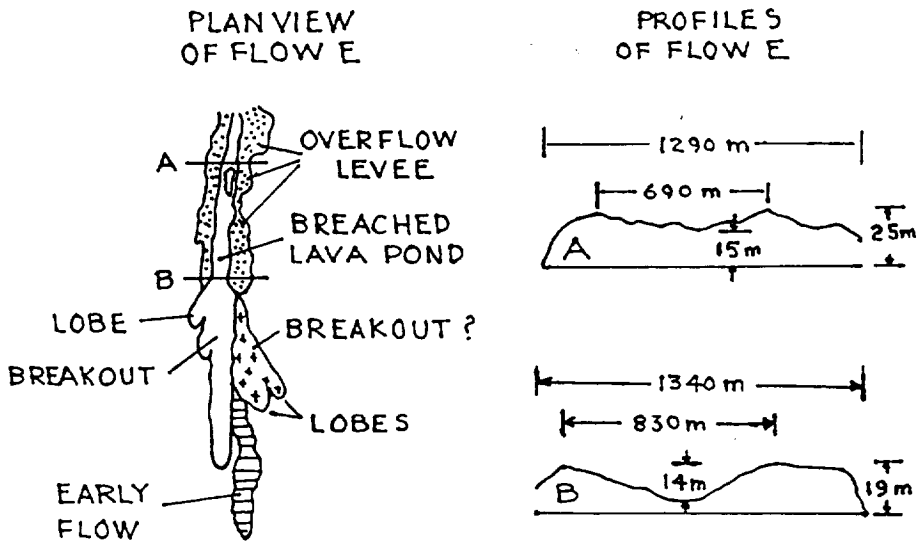

Figure 1. Plan view and photoclinometric profiles of Flow E of Zimbelman [2]. Profile B is same as E5 of Zimbelman [2]; Zy=15 m in Table 1 estimated from profile A.

Table 1. Comparison of dimensions and rheologies for profile E5 of Zimbelman [2] and this work. Equations used to calculate yield strengths (Y1, Y2, and Y3) and Bingham viscosities are given in Zimbelman [2].

Source	Flow Dimensions						Slope Angle	Effusion Rates	
	Zy m	Zl m	Zf m	Yc m	Yf m	Xf km	Theta deg.	Fc m^3/s	Fg m^3/s
Zimbelman	25	25	na	470	1350	14.8	5.0	59	
This work	15	19	29	830	1340	15.4	3.8	120	96

	Yield Strength (kPa)				Bingham Viscosity (Mpa) Graetz (Fc)			Cooling (Fc)		
	Y1[1]	Y2	Y3[2]	Y4[3]	E1[2]	E2[2]	E3[2]	Ew[1]	Eh[2]	E4[3]
Zimbelman	21	4	63		12	3	36			
This work	8	2	19	4	12		19	9	14	4

[1] Wide-flow model. [2] Hulme model. [3] Baloga and Crisp Model.

SURFACE-MATERIAL MAPS OF VIKING LANDING SITES ON MARS; H.J. Moore, U.S. Geological Survey, Menlo Park, CA, 94025; J.M. Keller, Stanford University, Stanford, CA, 94309.

We have mapped the surface materials at the Viking landing sites because a review of the literature reveals that such maps have not been made and better information on the types of materials and their abundances should lead to a better understanding of the geology and remote-sensing signatures of the sites. The maps extend to 9 m in front of each lander and are about 15 m wide -- an area comparable to the area of a pixel in the highest resolution Viking Orbiter images of the Lander 1 site.

The maps are divided into near and far fields. Data for the near fields are from: 1/10-scale maps [1], unpublished maps, and lander images. Data for the far fields are from: 1/20-scale contour maps [2], lander camera mosaics with overlain contours [2], and lander images. Rocks were located on these maps using stereometric measurements and the contour maps. Rocks form the control for delineation of other surface materials.

Map units are: (1) fine, (2) soillike, and (3) rock materials. Coordinates, length (l), width (w), and height (h) for each rock are recorded in a file for computational purposes. For many rocks, l or w was estimated. The rocks are assumed to be ellipsoids. Size-frequency and area-covered distributions of rocks are derived from the file according to the surrounding map unit, field, and size. All rocks mapped within fine material and all rocks >0.25 m in the near and far fields are included in the distributions, but rocks <0.25 m in the far fields are assumed to have the same distribution as rocks <0.25 m in the near fields. Areas covered by fine materials and rocks and soillike materials and rocks are measured on the maps. Areas covered by fine and soillike materials are obtained by subtraction of the area covered by rocks.

The forms of our size-frequency distributions of rocks are similar to previous ones [1,3]. Frequencies of rocks >0.18 m are larger at Lander 2 than Lander 1, but the reverse is true for smaller rocks. Fractions of area covered by the larger rocks in logarithmic size-bins are irregular and yield no simple relations for extrapolations to larger sizes of rocks, but the areas covered by small rocks diminish rapidly with decreasing size. Our fractions of area covered by centimeter-size and larger objects and rocks are about 11.5% at Lander 1 and about 16% at Lander 2. Outcrops of rock cover an additional 4.5% of the area at the Lander 1 site. At Lander 1, about 18% of the surface is covered by thick deposits of fines and 40% by both thick and thin fines. At Lander 2, about 30%

of the surface is covered with fine material.

Although there are questions about the physical properties of the materials mapped beyond the sample fields, we assume that the fine materials are loose fine-grained powders with a small thermal inertia like that previously assumed for drift material [4]. If this assumption is correct, our results suggest that the thermal inertias of crusty to cloddy and blocky materials [1] may be larger than previously estimated [4] and that the amounts of SO_3 plus chlorine in the soillike materials [5] are directly proportional to their thermal inertias. These differences do not substantially alter the previous conclusions of Moore and Jakosky [4].

Preliminary analyses of our data suggest that polarized- and depolarized radar-echo cross sections and normal radar reflectivities for the Lander 1 site should be about the same at 3.5- and 12.5-cm wavelengths. For Lander 2, polarized- and depolarized-echo cross sections are smaller and the quasi-specular cross section is larger at 3.5-cm wavelength than at 12.5-cm wavelength. These relations are chiefly related to the area distributions of rocks and the model used to calculate the radar cross sections [5,6]. For Lander 2, the fraction of area covered by "wavelength-size" rocks, or diffuse scatterers, is smaller for the 3.5-cm wavelength than the 12.5-cm wavelength; for Lander 1, these areas are about the same for both wavelengths. For Lander 2, the fraction of area of large rocks contributing to the quasi-specular echo is greater at the 3.5-cm wavelength than at the 12.5-cm wavelength; for Lander 1 these areas are about the same at both wavelengths. Finally, the three types of surface materials and "wavelength-size" rocks contribute to the bulk quasi-specular radar echoes in complicated ways.

REFERENCES

[1] Moore, H.J., et al., 1987, U.S. Geol. Prof. Paper 1389, 222p. [2] Liebes, S. Jr., 1982, NASA CR 3568, 290p. [3] Binder, A., et al., 1977, J. Geophys. Res., v. 82, p. 4439-4451. [4] Moore H.J. and Jakosky, B.M., 1989, Icarus, v. 81, p. 164-184. [5] Evans, J.V. and Hagfors, T., 1964, Icarus, v. 3, p.151-160. [6] Campbell, M.J. and Ulrichs, J., 1969, J. Geophys. Res., v. 74, p. 5867-5881.